Biophysical Journal Volume 71 November 1996 2380–2393

Single Neuron Local Rational Arithmetic Revealed in Phase Space of Input Conductances

Meng Wang and Chang N. Zhang
Department of Computer Science, University of Regina, Regina, Canada S4S OA2

ABSTRACT We present a phase space analysis to explore the potential of single neuron local arithmetic operations on its input conductances. This analysis was conducted first by deriving a rational function model of local spatial summation by using the equivalent circuits for steady-state membrane potentials. It is shown that developed functional phases exist in the space of input conductances, where a single neuron's local operation on input conductances can be described in terms of a set of well-defined arithmetic functions. It is further suggested that this single neuron local rational arithmetic is programmable, in the sense that the selection of these functional phases can be effectively instructed by presynaptic activities. This programmability adds the degree of freedom in a single neuron's ability to process the input information.

INTRODUCTION

During the past three decades, the classical view of single cortical neurons as simple summing machines of synaptic inputs has been significantly changed to include various nonlinear operations as elementary features of neuronal signal processing. Through the investigation into biophysical mechanisms of membrane potential dynamics, a number of arithmetic and logic operations have been proposed that can be performed by single neurons on their input conductances (Blomfield, 1974; Torre and Poggio, 1978; Koch et al., 1982; Shepherd and Brayton, 1987; Zador, et al., 1992; Mel, 1994; Carandini and Heeger, 1994). Most of these models have been inspired by certain required physiological properties of cortical neurons and have served as feasible explanations for some physiological functions that are hard to be accounted for by the classical linear summation model (Hubel and Wiesel, 1962; Marr, 1970; Blomfield, 1974; Torre and Poggio, 1978; Koch et al., 1982; Heeger, 1992, 1993).

The computational approach to single neuron functions focuses on the operational properties of membrane structures equipped with cross-membrane ionic pathways. In this approach, a computational model of single neurons looks at a set of admissible operations that can be supported by certain biophysical mechanisms, where the gated conductances are the operands and local postsynaptic potentials are the outcomes of the operations. This viewpoint defines a mapping from the space of the input conductances to the space of membrane potentials. Two types of models of this mapping can be identified: single mode and multiple mode. Previous models (Blomfield, 1974; Torre and Poggio, 1978; Koch et al., 1982; Shepherd and Brayton, 1987; Zador et al., 1992; Mel 1994; Carandini and Heeger, 1994) may be referred to as the single mode models in the sense that there is only one operation in the set of admissible operations. In other words, those models have defined exactly one operation (e.g., division) that can be performed by a given input configuration (e.g., a shunting conductance and an excitatory conductance). In contrast, multiple mode models would consider a set of multiple operations that can be performed in a given configuration. In this case, we perceive the space of input conductances to contain several well-defined (perhaps overlapping) phases such that different operations may be conducted when the values of inputs fall in different phases for a given input configuration.

In this work, we developed a phase-space analysis to derive a multiple mode model of neuronal local arithmetic. Specifically, we studied the phase structure of mapping from gated conductances to the local membrane potentials. Starting with a pavement of membrane using a simplified circuit model, a rational function model was formulated as a general relation between the gated conductances and postsynaptic potentials. Then, several forms of clean operations that approximate the rational function model were considered. The conditions for performing these clean operations led to a partition of the input conductance space into functionally distinct phases. A multiple mode model was finally established by verifying the developedness of those clean operations. Furthermore, by noting that all those clean operation modes were developed from a common general form, and therefore that they can turn to each other mode under the instruction of presynaptic activities, a concept of programmability of neuronal local arithmetic was proposed.

A complete electrical model of a membrane patch requires both the conductive and capacitive pathways to be considered. In this work, a simplified model consisting of only the conductive mechanisms was used. Dealing with such simplified models is equivalent to dealing only with the steady state of the membrane potentials. In slow synaptic events where the time window between successive open-

Received for publication 30 January 1996 and in final form 27 August 1996.

Address reprint requests to Dr. Chang N. Zhang, Department of Computer Science, University of Regina, Regina, Saskatchewan S4S OA2, Canada. Tel.: 306-585-4598; Fax: 306-585-4745; E-mail:zhang@cs.uregina.ca.

0006-3495/96/11/2380/14 $2.00

ing/closing of channels is remarkably larger than the membrane time-constant, the steady-state value corresponds to a peak of the membrane potential, and for a majority time of observation the membrane potential takes one of these peak values. In these circumstances, steady-state values and all statistical measurements based on them are physiologically significant (Kandel et al., 1991). By dropping the capacitive component, the governing equation of membrane potential dynamics becomes an algebraic equation, where it helps to find an explicit and closed-form representation of membrane potentials as functions of the gated conductances.

RATIONAL FUNCTION MODEL OF SPATIAL SUMMATION

General model

The membrane surface of a single neuron is considered as a segmentation, or a pavement, by membrane patches. So far as spatial summation is concerned, we consider the simplified circuit model of a passive membrane patch as shown in Fig. 1*a* where the capacitive pathway is removed. This patch model possesses a patch electromotive potential

$$V^m = \frac{g_m E_m + g_{sp} E_{sp}}{g_m + g_{sp}}, \tag{1}$$

which has a zero at $g_{sp}^0 = -g_m E_m / E_{sp}$ and no pole because $g_m > 0$ and $g_{sp} \geq 0$. Relation 1 can be regarded as a rational function when the potential-conductance relationship is considered.

Tangential-membrane interactions among patches are modeled by an axial resistance network. If the tangential-membrane current between patch i and patch j is significant (for instance, in the case of two adjacent dendritic patches), then an axial resistance r_{ij} is considered in the network that associates the equivalent circuits of patch i and patch j. Fig. 1 *b* illustrates the general equivalent circuit model corresponding to an arbitrary pavement geometry. Formally, the definition of patch electromotive potential given in relation 1 can be generalized: let V_i^m be the electromotive force of patch i, which is measured at the site of V_i in Fig. 1 *b* when patch i is isolated from the axial resistance network, and is evaluated according to relation 1. We define the inter-patch conductance G_{ij} as

$$G_{ij} = [(g_m + g_j)^{-1} + R_{ij}]^{-1}, \tag{2}$$

which is the conductance of patch j in a series with the conductance resistance R_{ij} evaluated in the open-circuit configuration in Fig. 1 *c* (in general $G_{ij} \neq G_{ji}$).

A pavement of the whole membrane by such membrane patches defines a set of n spatial summation values $\{V_1, V_2, \ldots, V_n\}$ measured at n sites on the membrane, where V_i is the cross-membrane potential observed at patch i when it is connected with the axial resistance network. Applying Kirchhoff's current law to the total current from all patches to the considered patch i, we have the following basic theorem of spatial summation:

Theorem

In an n-patch membrane pavement with a specific axial resistance network, the spatial summation V_i at any patch i is a weighted average of the patch electromotive potential of all patches, with the weighting factors given by the inter-patch conductances calculated from all individual patches to the patch i, respectively. Let V_i be the spatial summation at patch i, V_j^m be the electromotive potential of patch j, and G_{ij} be the inter-patch conductance between patches j and i; we then have

$$V_i = \frac{1}{\sum_j^n G_{ij}} \sum_j^n G_{ij} \times V_j^m, \quad i = 1, 2, \cdots, n. \tag{3}$$

In regard to the relation between patch electromotive potentials and spatial summations, Eq. 3 states a weighted-averaging model for spatial summation. However, for the relation between spatial summations and individual gated conductances, Eq. 3 represents a rational function model for spatial summation. In fact, by substituting Eqs. 1 and (2)

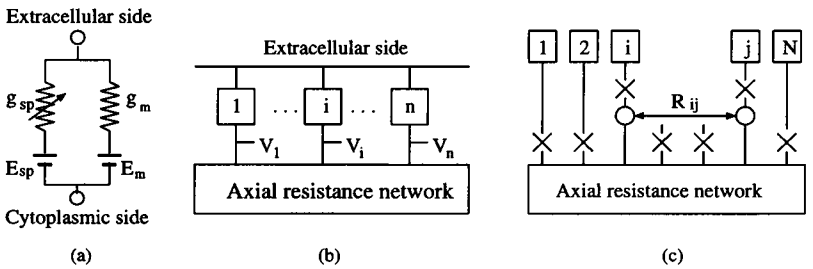

FIGURE 1 (*a*) The equivalent circuit model of a membrane patch used for calculation of spatial summation, showing the nongated and transmitted-gated pathways. E_{sp} is the reversal potential of synaptic potential, that is, $E_{sp} = E_{EPSP}$ for excitatory patches and $E_{sp} = E_{IPSP}$ for inhibitory patches. (*b*) The general circuit model corresponding to arbitrary pavement strategy. Spatial summation is measured at points $V_1, V_2, \ldots, V_n$. The extracellular environment is supposed to be of low resistance so that the extracellular side of the circuit is isopotential and is represented by a short circuit. The resting property of membrane is assumed uniform throughout all patches so that the values of g_m and E_m are the same everywhere. (*c*) Measurement of R_{ij}.

into Eq. 3, one has

$$V_i = \frac{\sum_j (E_m g_m + E_j g_j) \prod_{k\neq j}[1+R_{ik}(g_m + g_k)]}{\sum_j (g_m + g_j) \prod_{k\neq j}[1 + R_{ik}(g_m + g_k)]}, \quad i = 1, 2, \cdots, n. \tag{4}$$

This relation defines the spatial summation V_i as a rational function of the gated conductances $g_1, g_2, \ldots, g_n$. Both the numerator and the denominator of Eq. 4 are polynomials of the nth degree concerning $g_1, g_2, \ldots, g_n$. The degree of the polynomials in g_j ($j = 1, 2, \ldots, n$) is one. If we restrict ourselves to positive constitutive relations, then all coefficients, with the possible exception of E_j, are positive constant. The sign of E_j is determined in reference to the selection of E_m: if E_m is chosen to be -65 mV, then $E_j = E_{EPSP} = 0$ if patch j is excitatory and $E_j = E_{IPSP} = -70$ mV if patch j is inhibitory; if E_m is chosen to be zero, then $E_j = E_{EPSP} = 65'$ mV if patch j is excitatory and $E_j = E_{IPSP} = -5$ mV for inhibitory patches. Regardless of this selection, the rational function (Eq. 4) is analytical everywhere in its domain of definition. For typical cortical neurons, the values of conductances g_m and g_j are in the order of micromhos (10^{-6} S), and the axial resistances may range from near zero to several million ohms.

In the rational function (Eq. 4), it is easy to verify that V_i is a monotonic increasing (or decreasing) function of $g_j, j = 1, 2, \ldots$ if $E_j = E_{EPSP}$ (or E_{IPSP}). In fact, from the basic theorem (Eq. 3) we know that $\partial V_i/\partial V_j^m = G_{ij}/(\Sigma G_{ij}) > 0$, which means that V_i is an increasing function of patch electromotive potentials. On the other hand, one has from relation 1 that $\partial V_j^m/\partial g_j = g_m(E_j - E_m)/(g_m + g_j)^2$. Therefore, V_j^m is an increasing function of g_j when $E_j > E_m$ (i.e., when $E_j = E_{EPSP}$) and a decreasing function when $E_j < E_m$ (i.e., when $E_j = E_{IPSP}$).

It is well known that spatial summation saturates itself for large-valued gated conductances. This property is reflected in the rational function model by the fact that both the numerator and the denominator of Eq. 1 are of the same degree of $g_j, j = 1, \ldots, n$. To estimate the upper and lower bounds for the value of V_i, we notice that, from Eq. 3,

$$\min\{V_1^m, V_2^m, \cdots V_n^m\} \leq V_i \leq \max\{V_1^m, V_2^m, \cdots V_n^m\}. \tag{5}$$

Because relation 1 requires that

$$E_m \leq V_j^m < E_j, \quad \text{if} \quad E_j = E_{EPSP},$$

$$E_m \geq V_j^m > E_j, \quad \text{if} \quad E_j = E_{IPSP},$$

we have a looser relation:

$$\min\{E_m, E_1, E_2, \cdots, E_m\} \leq V_i \leq \max\{E_m, E_1, E_2, \cdots, E_n\}. \tag{6}$$

An even looser estimator follows that

$$E_{IPSP} < V_i < E_{EPSP}. \tag{7}$$

Local model

According to Eq. 2, if the axial resistance R_{pq} is extremely large for a pair of (p, q), then both G_{pq} and G_{qp} are small and so the mutual influence between patches p and q can be ignored. Theoretically we are able to detect and discard all such negligible G_{ij}'s in evaluating V_i ($i = 1, \ldots, n$), which results in n sets of admissible indices S_i ($i = 1, \ldots, n$) such that

$$V_i = \frac{1}{\sum_{j\in S_i}^n G_{ij}} \sum_{j\in S_i}^n G_{ij} \times V_j^m.$$

In all of the possible index sets $S_1, S_2, \ldots, S_n$, of interest is a partition of the index sets into the following groups

$$\{S_{l_1}, S_{l_2}, \cdots\}, \quad \{S_{p_1}, S_{p_2}, \cdots\}, \quad \cdots \quad \{S_{r_1}, S_{r_2}, \cdots\}$$

such that $S_l \cap S_p = \Phi$ where S_l and S_p belong to different groups. If such a partition can be constructed, then the spatial summations $V_1, V_2, \ldots, V_n$ can also be partitioned in the same manner:

$$\{V_{l_1}, V_{l_2}, \cdots\}, \quad \{V_{p_1}, V_{p_2}, \cdots\}, \quad \cdots \quad \{V_{r_1}, V_{r_2}, \cdots\}.$$

In this circumstance, patch electromotive potentials (and the spatial summations) in a specific group are related to each other, but are independent of the patch electromotive potentials and spatial summations in any other group. This is a situation where the single neuron activity contains several, relatively independent, local activity zones (Koch et al., 1982). This localization can proceed further for each of the groups until the following relation

$$V \approx \frac{\sum_j^B E_j g_j}{B * g_m + \sum_j^B g_j}. \tag{8}$$

becomes a good approximation to the original rational function (Eq. 4). Relation 8 is a zero-axial-resistance model for a local computation with B participating patches, where a unique spatial summation V is produced. We shall focus on the local model (relation 8) for the rest of this work.

PHASE SPACE OF LOCAL ARITHMETIC

All four basic arithmetic operations, including addition, subtraction, multiplication, and division, are involved in the rational function model (Eq. 4), whereas the multiplication is missing in the local model (relation 8). To what extent can the potential of these arithmetic operations on the gated conductances be realized through biologically plausible arrangement of parameters in the general model? To address this issue, we first considered the conditions under which the local model (relation 8) is reduced to various simple forms.

Basic arithmetic modes

A basic arithmetic mode is defined to be the case where the original rational function (Eq. 4) is approximated by a clean single arithmetic operation. For the well-definedness, two types of measure are used to characterize a clean arithmetic operation: 1) for a given $\epsilon > 0$, V is said to be approximated by a clean operation $g_1 \circ g_2$ in an area S in $g_1 - g_2$ plane, if for any $(g_1, g_2) \in S$ we have $|V - g_1 \circ g_2| < \epsilon$. S is referred to as the dynamic range of the operation $\circ$; 2) for a given S, the quantity $\eta = \max\{g_1 \circ g_2\} - \min\{g_1 \circ g_2\}$ $((g_1, g_2) \in S)$ is used to describe the value range of the operation $\circ$. We consider the following four types of clean operations.

Summation and subtraction

In these two clean operations, the low-axial-resistance operation (relation 8) is approximated by linear arithmetic:

$$V \approx \sum_j \left(\frac{E_j}{Bg_m}\right) g_j, \tag{9}$$

where summation takes place among the gated conductances of isopolarized patches and subtraction among heteropolarized patches. In the case of $B = 2$, the dynamic range S of the linear arithmetic is determined as follows (see Appendix A1):

Case I: $E_1 = E_2 \neq 0$ (additive mode):

$$0 < g_1 + g_2 < g_m[\epsilon + \sqrt{\epsilon(\epsilon + 4|E_1|)}]/|E_1|. \tag{10}$$

Case II: $E_1 > 0 > E_2$ (subtractive mode; the case of $E_2 > 0 > E_1$ can be known by symmetry): when $g_2 \geq g_m[\epsilon + \sqrt{\epsilon(\epsilon + 4|E_2|)}]/|E_2|$,

$$\sqrt{[g_2(|E_1| + |E_2|) - 2\epsilon g_m]^2 - 16\epsilon|E_1|g_m^2} - 2\epsilon g_m < 2|E_1|g_1 + (|E_1| - |E_2|)g_2 < \sqrt{[g_2(|E_1| + |E_2|) + 2\epsilon g_m]^2 + 16\epsilon|E_1|g_m^2} + 2\epsilon g_m, \tag{11}$$

and when $g_2 < g_m[\epsilon + \sqrt{\epsilon(\epsilon + 4|E_2|)}]/|E_2|$,

$$0 < 2|E_1|g_1 < \sqrt{[g_2(|E_1| + |E_2|) + 2\epsilon g_m]^2 + 16\epsilon|E_1|g_m^2} + 2\epsilon g_m - (|E_1| - |E_2|)g_2. \tag{12}$$

It is seen from Fig. 2 that the dynamic ranges for the two types of linear approximations possess different natures. In general, the additive mode is observed when both g_1 and g_2 are small in respect to the g_m (refer to relation 10). This observation is consistent with the general intuition that the linear approximation (Eq. 9) is valid in the small signal circumstances. Nevertheless, as can be seen from Fig. 2 *b*, the subtractive mode does not necessarily operate with small signals: the S of the subtractive mode occupies a narrow band expanding over a wide range in both g_1 and g_2 dimensions. The slope of this band can be well described by the ratio $|E_2|/|E_1|$. For $E_1 = 65$ and $E_2 = -5$, this indicates that the magnitude of the inhibitory conductance signal has to be around 13 times higher than the excitatory conductance signal to perform effectively a subtractive operation.

Multiplication

For $B = 2$, we consider the multiplicative approximation of relation 8 of the form

$$V \approx \frac{E_2}{4g_m^2} g_1 g_2. \tag{13}$$

The dynamic range of it is determined for three cases (see Appendix A2):

Case I: $E_1 = E_2 \neq 0$ (isopolarized multiplication):

$$4g_m^2(|E_1| - \epsilon) - |E_1|g_2(g_2 + 2g_m) + \sqrt{[4g_m^2(|E_1| - \epsilon) + |E_1|g_2(g_2 + 2g_m)]^2 - 32E_1^2g_m^3g_2} < 2|E_1|g_1g_2 < 4g_m^2(|E_1| + \epsilon) - |E_1|g_2(g_2 + 2g_m) + \sqrt{[4g_m^2(|E_1| + \epsilon) + |E_1|g_2(g_2 + 2g_m)]^2 - 32E_1^2g_m^3g_2}. \tag{14}$$

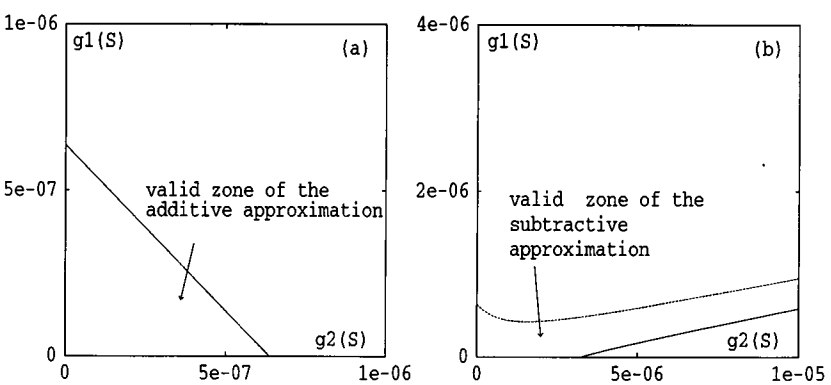

FIGURE 2 Dynamic range of the linear approximation in the case of (*a*) $E_1 = E_2 = E_{EPSP}$ and (*b*) $E_1 = E_{EPSP}$ and $E_2 = I_{EPSP}$. Parameters for the curves: $E_{EPSP} = 65$, $E_{IPSP} = -5$, $g_m = 10^{-6}$, $\epsilon = 5$.

Case II: $E_1 > 0 > E_2$ (heteropolarized multiplication):

$$\begin{aligned} &4g_m^2(|E_1| - \epsilon) - |E_2|g_2(g_2 + 2g_m) \\ &+ \sqrt{[4g_m^2(|E_2| - \epsilon) + |E_2|g_2(g_2 + 2g_m)]^2 - 32E_2^2g_m^3g_2} \\ &< 2|E_2|g_1g_2 < 4g_m^2(|E_1| + \epsilon) - |E_2|g_2(g_2 + 2g_m) \\ &+ \sqrt{[4g_m^2(|E_2| + \epsilon) + |E_2|g_2(g_2 + 2g_m)]^2 - 32E_2^2g_m^3g_2}. \end{aligned} \tag{15}$$

Case III: $E_1 = 0$, $E_2 \neq 0$ (shunting multiplication):

$$\begin{aligned} &\sqrt{[g_2|E_2|(g_2 + 2g_m) - 4\epsilon g_m^2]^2 + 16(g_mg_2|E_2|)^2} \\ &- [|g_2|E_2|(g_2 + 2g_m) + 4\epsilon g_m^2] < 2|E_2|g_1g_2 \\ &< \sqrt{[g_2|E_2|(g_2 + 2g_m) + 4\epsilon g_m^2]^2 + 16(g_mg_2|E_2|)^2} \\ &- [|g_2|E_2|(g_2 + 2g_m) - 4\epsilon g_m^2]. \end{aligned} \tag{16}$$

Fig. 3 illustrates the dynamic ranges of the multiplicative mode (Eq. 13) in isopolarized, heteropolarized, and shunting cases. In both the isopolarized and heteropolarized cases, the S is a narrow band bounded by two curves (not strictly hyperbolic; see relations 14 and 15). When one of the two patches is of the shunting type, the shunting conductance g_1 can vary in a wide range for small g_2 and this range becomes more narrow as the shunted conductance increases (Fig. 3 *c*).

Division

In relation 8, suppose that the index set $\{j\}$ is partitioned into two nonoverlapping subsets $\{k\}$ and $\{l\}$ such that

$$V \approx \frac{\sum_k^K E_kg_k + \sum_l^L E_lg_l}{B * g_m + \sum_k^K g_k + \sum_l^L g_l} \tag{17}$$

where $K + L = B$. A divisive approximation of relation 8 takes the form of

$$V \approx \frac{\sum_k^K E_kg_k}{B \times g_m + \sum_l^L g_l}, \tag{18}$$

that is, the conductances corresponding to the subset $\{l\}$ effectively divide the conductances in the subset $\{k\}$. For the case of $B = 2(L = K = 1)$, the rational function $(E_1g_1 + E_2g_2)/(g_1 + g_2 + 2g_m)$ is approximated by $E_2g_2/(g_1 + 2g_m)$, for which the dynamic range is determined as follows (see Appendix A3).

Case I: $E_1 = E_2 \neq 0$ (isopolarized division):

$$\begin{aligned} &\frac{-[\epsilon(g_2 + 4g_m) + 2g_m|E_1|] + \sqrt{[2g_m|E_1| - \epsilon g_2]^2 + 4|E_1|(|E_1| + \epsilon)g_2^2}}{2(|E_1| + \epsilon)} \\ &< g_1 < \frac{\epsilon(g_2 + 4g_m) - 2g_m|E_1| + \sqrt{[\epsilon g_2 + 2g_m|E_1|]^2 + 4|E_1|(|E_1| - \epsilon)g_2^2}}{2(|E_1| - \epsilon)}. \end{aligned} \tag{19}$$

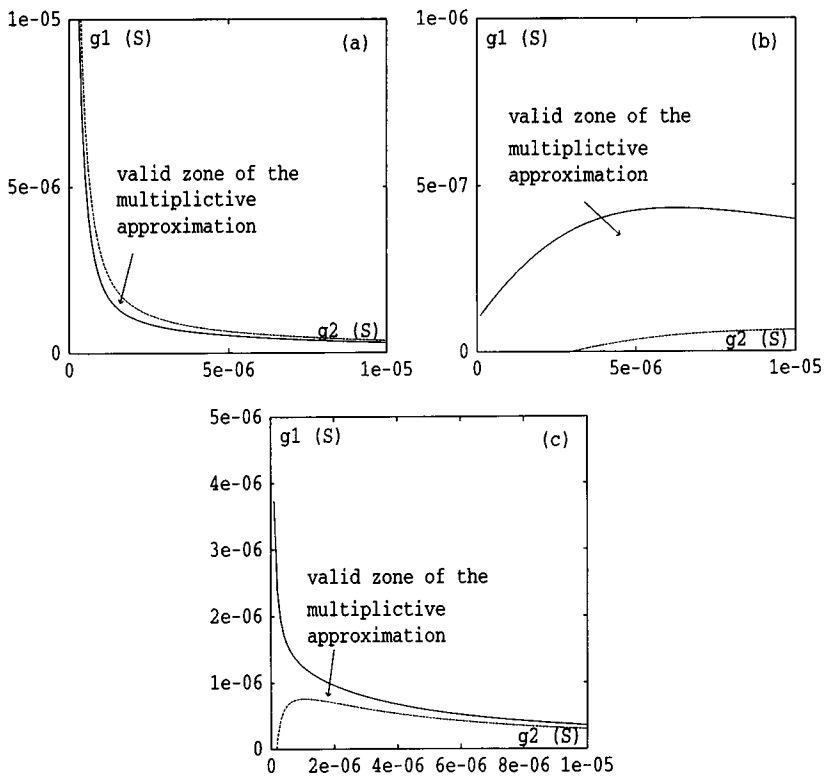

FIGURE 3 Dynamic range of the multiplicative approximation in the case of (*a*) $E_1 = E_2 = E_{EPSP}$, (*b*) E_1 = EPSP and E_2, = E_{IPSP}, and (*c*) $E_1 = 0$ and $E_2 = E_{EPSP}$. Parameters for the curves: $E_{EPSP} = 65$, $E_{IPSP} = -5$, $g_m = 10^{-6}$. For (*a*) and (*c*), $\epsilon = 5$. For (*b*), $\epsilon = 3$.

Case II: $E_1E_2 < 0$ (heteropolarized division):

$$0 \le g_1 < \frac{\epsilon(g_2 + 4g_m) - 2g_m|E_1| + \sqrt{[\epsilon g_2 + 2g_m|E_1|]^2 - 4|E_2|(|E_1| - \epsilon)g_2^2}}{2(|E_1| - \epsilon)},$$

$$0 \le g_2 \le \frac{g_m|E_1|}{\sqrt{|E_2|(|E_1| - \epsilon) - 0.5\epsilon}}. \quad (20)$$

Case III: $E_1 = 0$ and $E_2 \neq 0$ (shunting division):

$$g_1 > g_2[\sqrt{0.25 + |E_2|/\epsilon} - 0.5] - 2g_m. \quad (21)$$

The S of the isopolarized division is shown in Fig. 4 *a*. Similar to the case of subtraction, the S is a narrow band, but with a slope of almost one. There are two possibilities with the case of $E_1E_2 < 0$, that is, $E_1 > 0 > E_2$ (Fig. 4 *b*) and $E_1 < 0 < E_2$ (Fig. 4 *c*). For both of them, the S is stretched along the dimension of the inhibitory conductance. The S of the shunting division occupies one half of the $g_1 - g_2$ plane, indicating a very loose restriction to be met by the two participating conductances to perform a division.

Because of the monotonity of the rational function (relation 8) and of its various approximations (Eqs. 9, 13, and 18) it suffices to determine the value range of each of the basic modes by looking at the function value on the boundaries of the S. For the additive mode and the shunting divisive mode, it is readily known that $\eta = [\epsilon + \sqrt{\epsilon(\epsilon+4|E_1|)}]/2$. With $\epsilon = 5$, it gives 20.7 mV for $E_1 = 65$ (EPSP) and 8.1 mV for $E_1 = -5$ (IPSP). Fig. 5 illustrates the value ranges of other basic modes. It is noteworthy that for the cases of subtractive (Fig. 5 *a*), isopolarized (Fig. 5 *b*) and shunting multiplicative (Fig. 5 *d*), and isopolarized divisive (Fig. 5 *e*) modes, although their the dynamic ranges are narrowly bounded (see Figs. 2 *b*, 3, *a* and *c*, and 4 *a*), their value ranges are broad. Divisive mode for the case of $E_1E_2 < 0$ has two realizations: $E_1 > 0 > E_2$ and $E_1 < 0 < E_2$. In the former the quotient is purely negative, whereas in the latter the quotient is positive. The original rational function (relation 8) can take both positive and negative values in the area of S (Fig. 5, *f* and *g*).

Phase diagram of arithmetic modes

Based on the identification of the four basic arithmetic modes, phase diagrams can be achieved for three types of polarization configurations: 1) two isopolarized patches, 2) two heteropolarized patches, and 3) a shunting patch and an excitatory (or inhibitory) patch. Phase diagrams (Fig. 6) prescribe a restriction on what types of arithmetic can be performed by a specific polarization configuration. As can be seen from Fig. 6, two isopolarized patches can effectively perform addition, multiplication, and division, but no subtraction (Fig. 6 *a*); two isopolarized patches may perform subtraction, multiplication, and (a little) division (Fig. 6 *b*); finally, multiplication and division are two typical operations with the shunting configuration (Fig. 6 *c*). There are overlaps between some

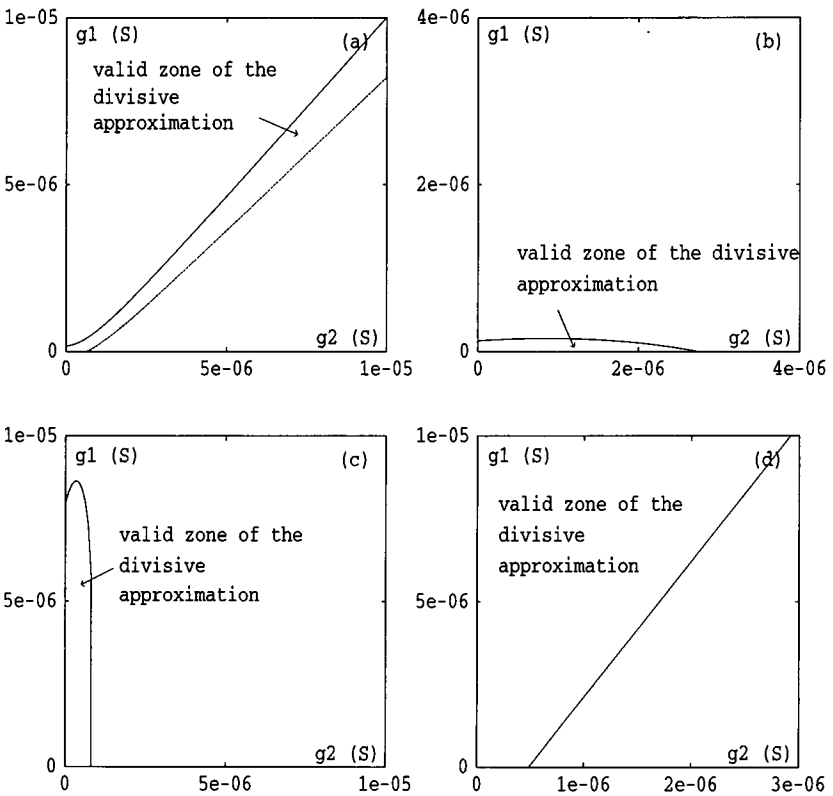

FIGURE 4 Dynamic ranges of the divisive approximation. (*a*) When $E_1 = E_2 = E_{EPSP}$. (*b*) $E_1 = E_{EPSP}$ and $E_2 = E_{IPSP}$. (*c*) $E_1 = E_{IPSP}$ and $E_2 = E_{EPSP}$. (*d*) When $E_1 = 0$ and $E_2 = E_{EPSP}$. Parameters for all curves: $E_{EPSP} = 65$, $E_{IPSP} = -5$, $g_m = 10^{-6}$, $\epsilon = 5$.

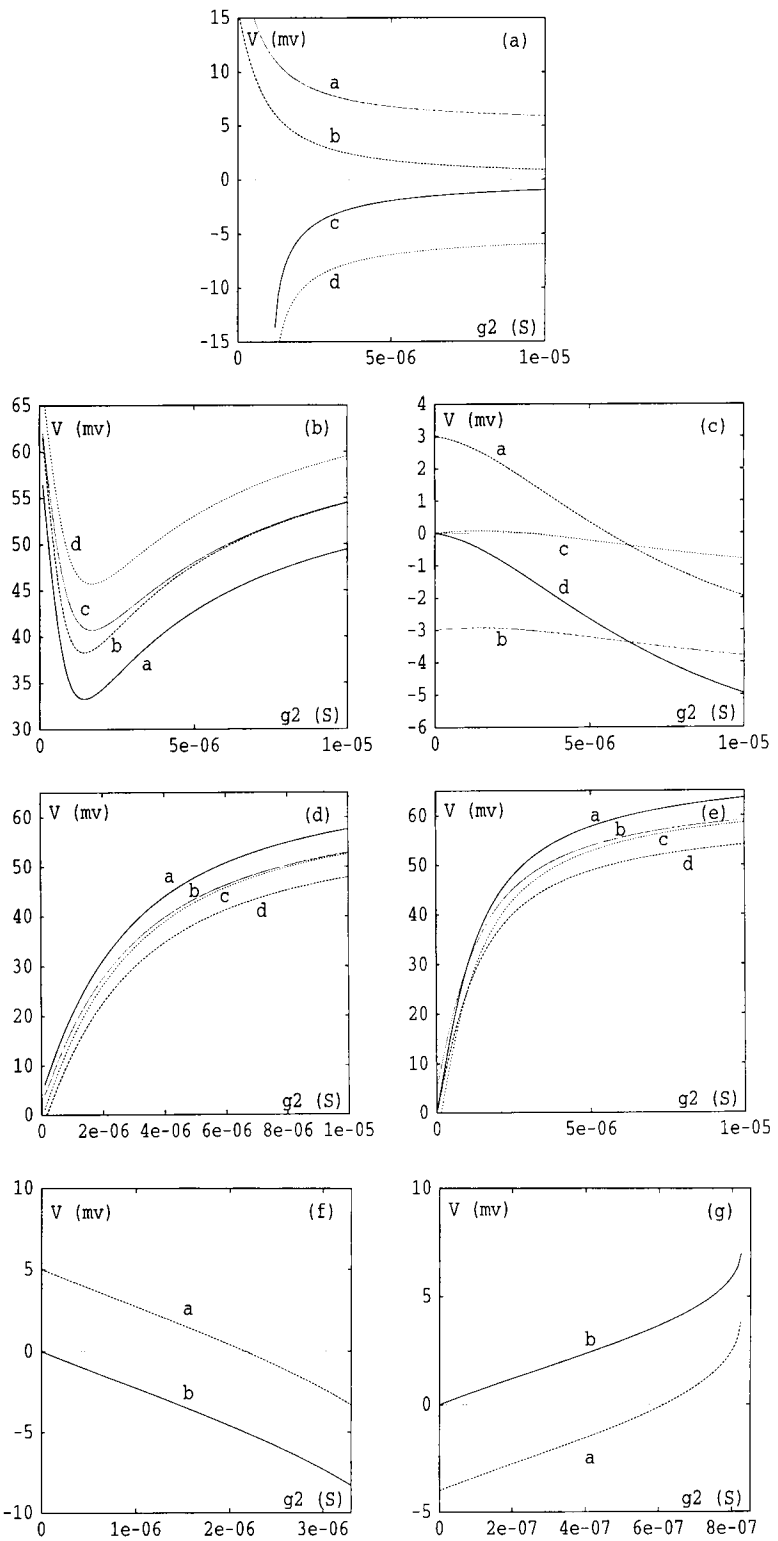

FIGURE 5 Value ranges of the basic arithmetic modes shown as functions of g_2. (*a*) Subtractive mode with $E_1 = E_{EPSP}$ and $E_2 = E_{IPSP}$. Curves *b* and *c*: upper and lower bounds of the subtractive approximation. Curves *a* and *d*: original rational function (4) evaluated on the upper and lower boundaries of the dynamic range, respectively (see Fig. 2*b*). (*b*)–(*d*) Multiplicative mode with (*b*) $E_1 = E_2 = E_{EPSP}$, (*c*) $E_1 = E_{EPSP}$ and $E_2 = E_{IPSP}$, and (*d*) $E_1 = 0$ and $E_2 = E_{EPSP}$. (*b*) Curves *a* and *d*: lower and upper bounds of the multiplicative approximation. Curves *b* and *c*: original rational function evaluated on the lower and upper bounds of the dynamic range, respectively (see Fig. 3*a*). (*c*) Curves *c* and *d*: upper and lower bounds of the multiplicative approximation. Curves *a* and *b*: original rational function evaluated on the upper and lower boundaries of the dynamic range, respectively (Fig. 3*b*). (*d*) Curves *a* and *d*: upper and lower bounds of the multiplicative approximation. Curves *b* and *c*: original rational function evaluated on the lower and upper boundaries of the dynamic range, respectively (Fig. 3*c*). (*e*)–(*g*) Divisive mode with (*e*) $E_1 = E_2 = E_{EPSP}$, (*f*) $E_1 = E_{EPSP}$ and $E_2 = E_{IPSP}$, and (*g*) $E_1 = E_{IPSP}$ and $E_2 = E_{EPSP}$. (*e*) Curves *a* and *d*: upper and lower bounds of the divisive approximation. Curves *b* and *c*: original rational function evaluated on the upper and lower boundaries of the dynamic range, respectively (refer to Fig. 4*a*). (*f*) Curve *b*: upper bound of the divisive approximation. Curve *a*: original rational function evaluated on the upper boundary of the dynamic range (Fig. 4*c*).

phases, indicating that for certain input values the arithmetic function of the system may be interpreted in a number of ways. The areas not marked with specific functions correspond to the general rational function (relation 8).

IMPLICATION TO PHYSIOLOGICAL FUNCTIONS

In the last section we have constructed the phase space for two-patch systems. In group operations that usually involve more than two varying conductances, composite arithmetic

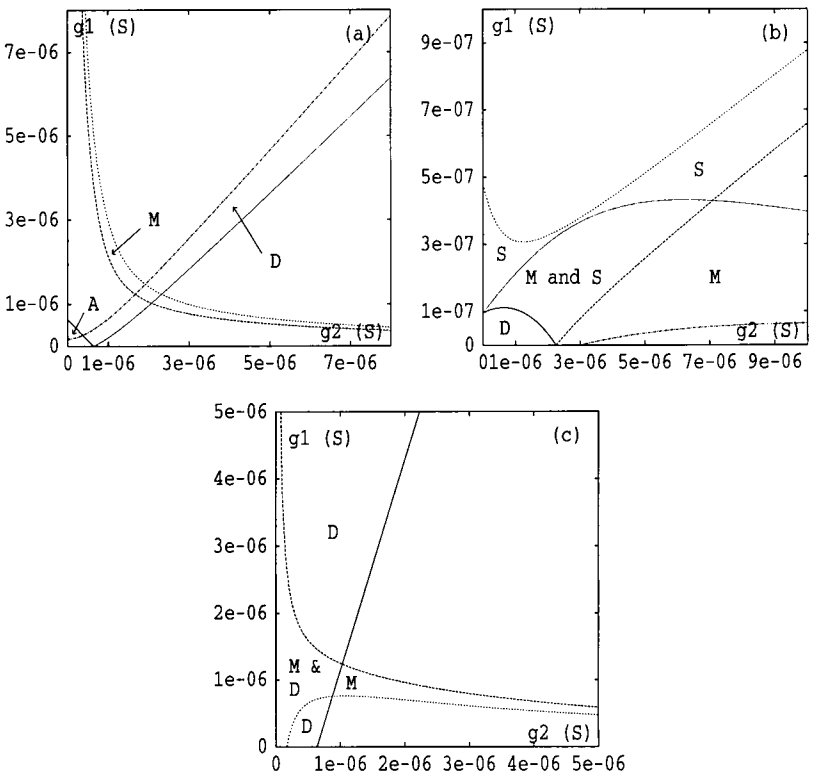

FIGURE 6 (*a*) Three-phase diagram of the system of two isopolarized patches in $g_1 - g_2$ plane. (*b*) Three-phase diagram of the system of two heteropolarized patches. (*c*) Two-phase diagram of the system of a shunting patch and an excitatory patch. A: additive phase; S: subtractive phase; M: multiplicative phase; D: divisive phase.

operations can be observed. Some of these operations are 1) Eq. 18: division-after-addition/subtraction; 2) $V = [\Sigma_{\{k\}}\ E_k g_k][\Sigma_{\{j\}}\ E_j g_j]$: multiplication-after-addition ($\Pi\Sigma$ operation); 3) $V = \Sigma_{i,\ j}\ E_j g_i g_j$: addition-after-multiplication ($\Sigma\Pi$ operation), and so on. The dynamic range and value range of these composite operations can be determined. For instance, for Eq. 18 with shunting denominator ($E_l = 0$ for all l), the dynamic range is given by

$$\sum_l g_l > \sqrt{0.25(\sum_k g_k)^2 + (\sum_k g_k)|\sum_k E_k g_k|/\epsilon} - 0.5\sum_k g_k - Bg_m. \tag{22}$$

The local computation model we have developed above under the zero-axial-resistance condition may serve as a point neuron model. When such model neurons are embedded into a specific neural circuit, certain physiological functions can be simulated. As an example, we consider a normalization model for simple cells in the primate visual cortex (Heeger, 1992; Carandini and Heeger, 1994). According to this model, a simple cell's response begins with a linear stage, which performs essentially the same function as in the linear summation model, followed by a normalization stage (Fig. 7 *a*). At the normalization stage, each cell's linear response is divided by a quantity proportional to the pooled activity of other cortical cells (Heeger, 1992; Carandini et al., 1994). The mechanism underlying the normalization model has been considered (Carandini et al., 1994) in terms of the equivalent circuit model of a isopotential membrane (see Fig. 7 *b*). The $E_{leak} - g_{leak}$ branch corresponds to the $E_m - g_m$ branch in our work; the two gated conductances g_e and g_i represent excitatory and inhibitory lateral Geniculate nucleus (LGN) contributions, respectively; and the gated channel g_{shunt} represents lateral interaction within the visual cortex. The steady-state value of membrane potential V is calculated as $V = I_d/g$, with

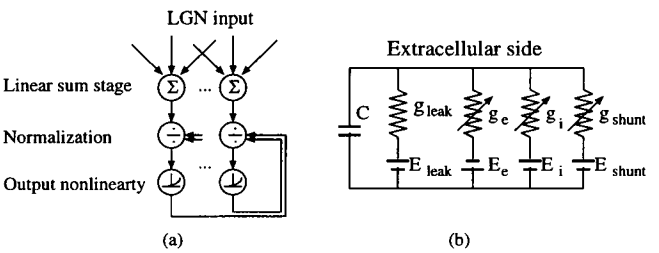

FIGURE 7 Heeger normalization. (*a*) Diagram of the normalization model. (*b*) Equivalent circuit model used by (Carandini, M., and D. Heeger 1994) to explain the membrane mechanism of normalization (adapted from Carandini and Heeger (1994)).

$$I_d = g_e E_e + g_i E_i + g_{shunt} E_{shunt} + g_{leak} E_{leak},$$

$$g = g_e + g_i + g_{shunt} + g_{leak}.$$

It was postulated (see Carandini et al., 1994) that g_e and g_i act as "linear synaptic conductances" and g_{shunt} as "normal-

ization synaptic conductance." By setting

$$g_i + g_e + g_{leak} = \text{const}, \quad (23)$$

$$E_{shunt} = 0, \quad (24)$$

the membrane potential V can be approximated as $V \approx (g_e E_e + g_i E_i + \text{const})/(g_{shunt} + \text{const})$, which effectively states that the linear summation $g_e E_e + g_i E_i$ of LGN inputs is divided by pooled cortical activity (the g_{shunt} term). This model can explain a variety of physiological phenomena (Heeger, 1992, 1993). However, there are difficulties in proposing biologically plausible mechanisms for the key assumption Eq. 23. As conductances are nonnegative, it is not plain to see how g_i and g_e trade off against each other.

If we interpret group K as the input from the LGN, group L as the pooled cortical activity, then our relation 18 restates the normalization model given by Heeger et al., the constant $B \times g_m$ in the denominator corresponding to the semisaturation constant (Heeger, 1992, 1993). The difficulty in the explanation of the assumption Eq. 23 can be overcome by our model: for a given ϵ, the model neuron can effectively perform Eq. 18 as long as the participating afferents meet relation 22. As we have seen in the case of $B = 2$, this relation specifies a half plane in the phase space of conductances as admissible conductance values, it can be easily satisfied by a large set of configurations.

Table 1 lists some dynamic ranges for the normalization model. The ratio $\Sigma_k g_k/B \times g_m$ reflects the total activity level of LGN input in respect to the resting level; the ratio $|\Sigma_k E_k g_k|/\Sigma_k g_k$ indicates the average membrane potential change induced by LGN input; and the ratio $\Sigma_l g_l/\Sigma_k g_k$ describes the level of intracortical activity in comparison to the LGN activity. As seen from Table 1 (row one), when the LGN input activity level is 50% as much as the resting level and the average LGN contribution to membrane potential is 6 mV, then the cell will perform a nice normalization operation ($\epsilon = 1$) for any nonzero intracortical activities. With the same level of intracortical activity (row two), if the LGN input is intensified to the same level as the resting level, then the required LGN-contributed membrane potential change is only 2 mV (allowing more inhibitory patches to be involved). At the same LGN activity level (rows four and five), if there are more excitatory patches involved, then a higher level of intracortical activity is needed to maintain the same level of operational accuracy. As a worst-case estimate, the last row of Table 1 presents the case where the LGN-contributed membrane potential change reaches the peak of 65 mV (all patches are excitatory) and the LGN input level is 10 times as much as the resting level; in this case, the ratio between the intracortical and LGN input activity levels is 7.48. A numerical simulation result is illustrated in Fig. 8.

TABLE 1 Dynamic ranges of the normalization model

ϵ	$\Sigma_k g_k/B \times g_m$	$\lvert\Sigma_k E_k g_k\rvert/\Sigma_k g_k$	$\Sigma_l g_l/\Sigma_k g_k$
1.00	0.50	6.00	>0.00
1.00	1.00	2.00	>0.00
1.00	2.00	0.75	>0.00
1.00	1.00	4.00	>0.56
1.00	1.00	8.00	>1.37
1.00	10.00	65.00	>7.48

DISCUSSION

Well-developedness of the arithmetic modes

Some previous works have suggested the existence of certain types of neuronal clean arithmetics. Blomfield (1974) has derived three types of operations: isopolarized addition (with small conductance changes), heteropolarized subtraction (with small conductance changes), and heteropolarized division (with large inhibitory conductance). Another work (Torre and Poggio, 1978) proposed a possible mechanism for shunting multiplication. Because their derivation is based on Taylor expansion of the original rational function, the result of (Torre and Poggio, 1978) applies only to small conductance circumstances, and some additional procedures are required to remove the unwanted terms in the expansion to give a clean multiplication (Poggio and Torre, 1981; Koch and Poggio, 1992).

By systematically exploring the phase space of the gated conductances, these established observations are verified and extended. As shown in Fig. 6, a total of eight phases can be observed in the three possible polarization configurations. All these clean operation modes can be described in three categories: less-developed, developed, and well-developed. A mode is called developed if it has a wide dynamic range (compared with g_m) in at least one dimension; it is well developed if, in addition, the dynamic diagram occupies a large portion of the phase space; and it is less developed if the dynamic range is narrow in both dimensions. Therefore, subtraction is found to be a developed mode for its broad dynamic range in both g_1 and g_2 dimensions (Fig. 6 *b*) together with its wide dynamic range (Fig. 5 *a*); and it is not well developed because of the limited phase area. As an extension to Blomfield's observation, it is evident from the phase diagram that the subtraction works not only for small conductance changes but also for large changes. The feature of a long, narrow band of the subtraction phase suggests that it is the interrelation between the two conductances, rather than the magnitude, that is important for the formation of a subtractive operation. Being also a linear operation, the addition is a less developed mode due to the narrow dynamic range in both dimensions (smaller than g_m). These two linear modes are so dissimilar in their phase diagrams that it is reasonable to consider them as two functionally different modes.

The multiplicative mode is developed in all three configurations. The isopolarized and shunting multiplications possess a wide dynamic range in both g_1 and g_2 dimensions (Fig. 6, *a* and *c*), whereas the heteropolarized multiplication is widely defined only in the g_2 dimension. The value range of the isopolarized and shunting multiplications is wide

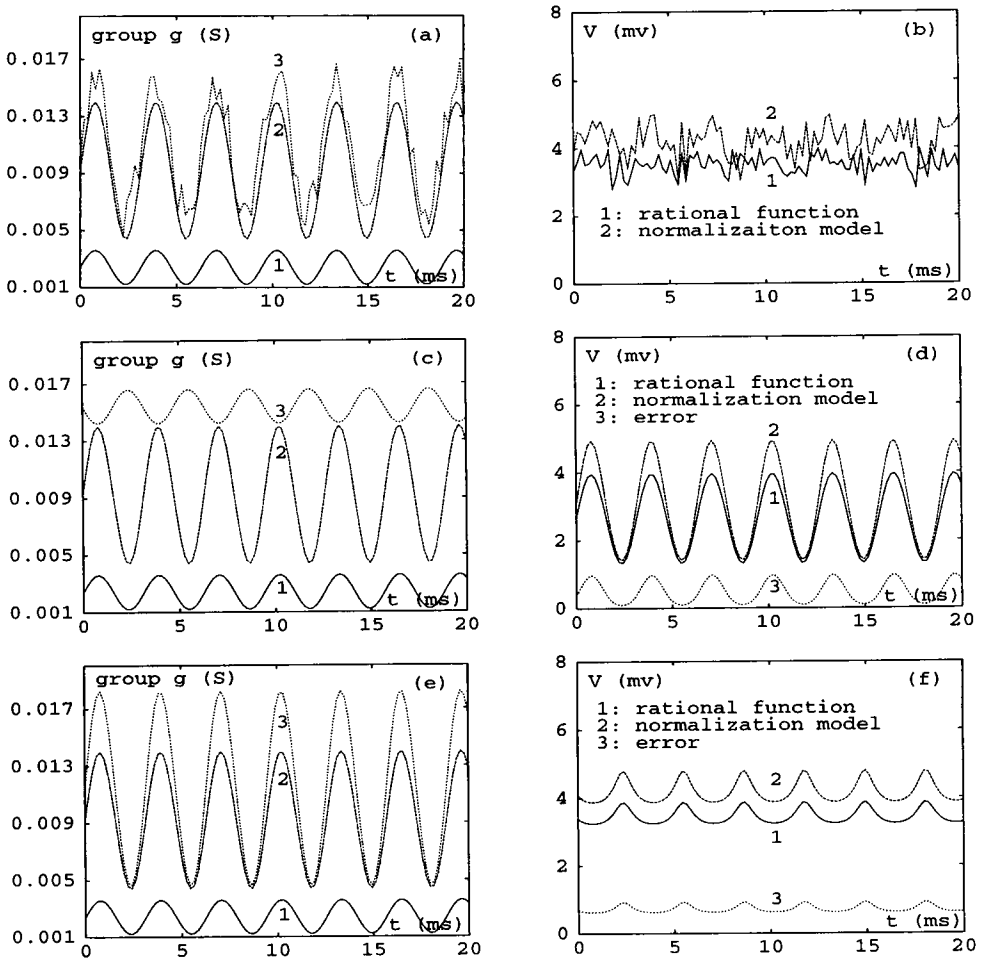

FIGURE 8 Simulation of the normalization model. A total of 400 patches is used, and the average LGN contribution to membrane potential is set to 20 mV. In *a*, *c*, and *e*, a hypothetic sinusoidal temporal pattern of LGN activity $\Sigma_k g_k$ is shown as curve 1, the lower bound for intracortical activity level as determined by Eq. 22 is shown as curve 2, and an admissible intracortical activity is shown as curve 3. Intracortical activity is determined in (*a*) by the bound (Eq. 22) plus white noises, in *c* as an oppositely phased temporal pattern, and in *e* as an in-phase pattern. The corresponding original rational model and the normalization model are depicted on the right. For all curves, $\epsilon = 1$.

(Fig. 5, *b* and *d*). In contrast, heteropolarized multiplication has a narrow value range (Fig. 5 *c*). It is worth noting that the phase diagrams of the isopolarized and shunting multiplications possess (not strictly) a hyperbolic nature that, as we shall see below, implies important restrictions on the activity patterns of g_1 and g_2.

Division is also observed in all three configurations. As judged from the small dynamic range (Fig. 4 *b*), the heteropolarized division of the excitatory-divides-inhibitory type is a less developed mode. On the other hand, the division of the inhibitory-divides-excitatory type can be observed for a large range of inhibitory conductance value (Fig. 4 *c*), suggesting that it is a developed mode (this is consistent with Blomfield's study). The isopolarized division is a developed mode (Fig. 5 *e* and Fig. 6 *a*) and has a narrow phase band similar to the case of subtraction.

In all of the eight possible modes, the shunting division is the only well-developed mode. This is evident from its broad dynamic range (Fig. 6 *c*) and large phase area (a half-phase plane). It also has a wide value range ($\eta = [\epsilon + \sqrt{\epsilon(\epsilon + 4|E_1|)}]/2$), which is independent of the value of the two conductances.

The developedness of each arithmetic mode is summarized in Table 2. The developedness of an arithmetic mode implies the physiological observability of the mode. Thus, the well-developedness of the shunting division suggests it to be a mostly observable physiological phenomenon. The developed modes can be observed under certain conditions. In general, less developed modes correspond to rare behaviors. However, as we shall see below, addition can be an observable mode when the cell's electrical activity is sustained at a low level.

Dependence on presynaptic activity

The phase diagrams in Fig. 6 divide the input space into functional areas: given an accuracy ϵ, an arbitrary conductance pair (g_1, g_2) may be said to carry out a general rational operation, a clean arithmetic, or several types of clean arithmetics (in the case of overlapped phases). Physiologically significant situations are those where the conductance pair (g_1, g_2), though changing, remains to stay in a specific phase for a remarkable time period such that a persistent clean operation is performed. For time-varying g_1 and g_2, this requirement implies that it is not the magnitude but the temporal pattern of conductance changes that is relevant to the triggering of a specific arithmetic mode.

TABLE 2 Developedness of arithmetic modes

Mode	Range in g_1	Range in g_2	Phase area	Developedness
Addition	Narrow	Narrow	Small	Less-developed
Subtraction	Wide	Wide	Small	Developed
Isopolarized multiplication	Wide	Wide	Small	Developed
Heteropolarized multiplication	Narrow	Wide	Small	Developed
Shunting multiplication	Wide	Wide	Small	Developed
Isopolarized division	Wide	Wide	Small	Developed
Heteropolarized division (inhibitory/excitatory)	Narrow	Narrow	Small	Less-developed
Heteropolarized division (excitatory/inhibitory)	Wide	Narrow	Small	Developed
Shunting division	Wide	Wide	Large	Well-developed

From Fig. 6, it is seen that the persistent triggering of the isopolarized multiplication and division, of the heteropolarized subtraction, and of the shunting multiplication (with large shunted conductance in respect to the g_m), demands highly ordered (g_1, g_2) activity patterns. Specifically, in-phase (g_1, g_2) temporal patterns may effectively trigger isopolarized division and heteropolarized subtraction, and oppositely phased (g_1, g_2) patterns may trigger a multiplication. Take the sinusoidal g_2 as example. It can be derived from relations 14, 19, and 11 that the most effective pattern of g_1 is a synchronized one with a phase difference of π for the multiplication and of zero for the division and the subtraction (Fig. 9).

Some clean arithmetics, such as addition and shunting division, do not require highly ordered input patterns. Addition is performed whenever the both gated conductances are small in respect to g_m. This condition associates the addition mode with the spontaneous synaptic activities, which are typically low-level and randomly phased. The shunting division does not require a well organized input, either. This nature, together with the large phase area the shunting division occupies in the phase space, suggests it to be a mostly observable functional state in the shunting configuration.

Strategy of single neuron arithmetics

Based on the above analysis, the strategy followed by single neuron arithmetic functions can be summarized for different configurations. Because of the high axial resistances, basic arithmetic operations are generally performed in local areas. For a local area consisting of mainly isopolarized patches, if the presynaptic activity level is low, then linear addition may be performed; if the presynaptic activity level is large and is in-phase synchronized, then division is performed; with high-level, oppositely phased presynaptic activities, multiplication is performed. In the local area consisting of isopolarized patches, low-level presynaptic activity may

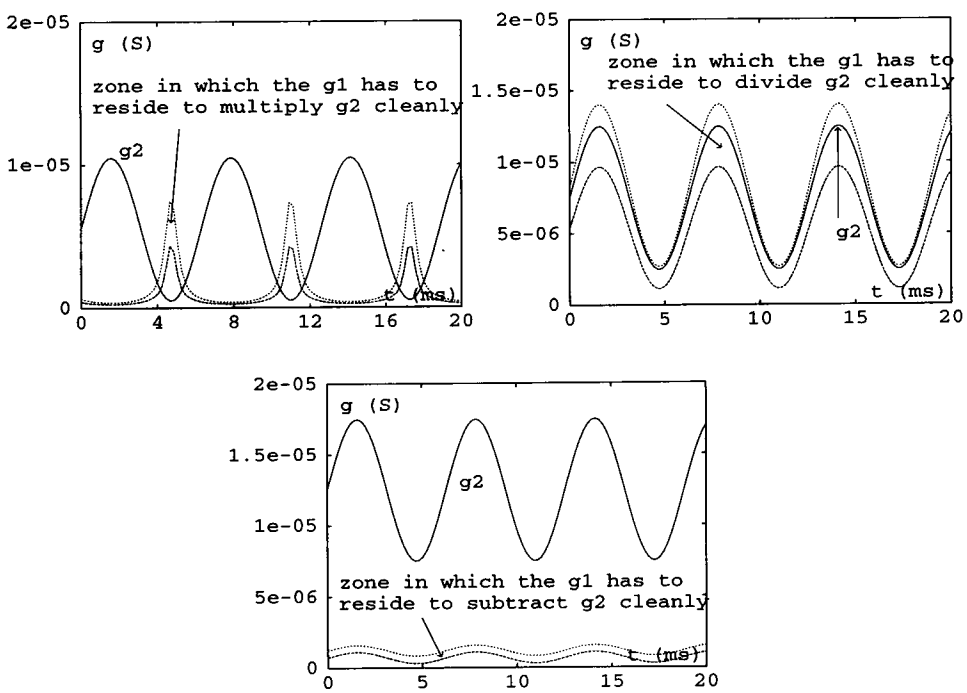

FIGURE 9 Temporal relationships between g_1 and g_2 for triggering a specific clean arithmetic. Given the sinusoidal pattern of g_2, the admissible range of g_1 is determined by relations 14, 19, and 11. (*a*) In the case of isopolarized multiplication, patterns of g_2 and g_1 are shown to possess a phase difference of π. In-phase synchronized patterns are observed in (*b*) for isopolarized division and (*c*) for heteropolarized subtraction. In all figures, ϵ is enlarged to 10 to show the close-up of the admissible zone for g_1.

effectively evoke division, subtraction, and multiplication, and high-level in-phase activity would trigger subtraction. For local areas rich in shunting patches, high-level oppositely phased presynaptic activities can produce multiplications, and sufficiently high-level activities in shunting patches can produce divisions.

In general, an ideal general-purpose arithmetic mechanism is required to possess a wide dynamic range and a wide value range. In this sense, single neurons and their computational dendrites are not good general-purpose arithmetic computers. However, it is this lack of generality that makes the single neurons and their computational subunits good programmable special-purpose computers. We have shown that the input space of single neurons can be divided into functional phases based on their arithmetic modes. Furthermore, transitions between functional phases are instructed by presynaptic activity. All these properties suggest single cortical neurons to be programmable rational approximators. Because there are a remarkable number of free parameters in the rational model, it is reasonable to expect more computational functions in the proposed model than what can be achieved by neuronal polynomial approximators (Poggio and Girosi 1990; Dubin and Rumelhart 1990; Mel and Koch 1990).

APPENDIX

In the following we assume that $\epsilon > 0$ is sufficiently small in comparison to $\min\{|E_1|, |E_2|\}$ for nonzero E_1 and E_2.

A1. Dynamic range of linear modes

The general form of the error is:

$$\left|\frac{E_1g_1 + E_2g_2}{g_1 + g_2 + 2g_m} - \frac{E_1g_1 + E_2g_2}{2g_m}\right| = \frac{(g_1 + g_2)|E_1g_1 + E_2g_2|}{2g_m(g_1 + g_2 + 2g_m)} \le \epsilon. \quad (25)$$

Case I

$E_1 = E_2 \neq 0$. The error (Eq. 25) takes the form

$$\frac{|E_1|(g_1 + g_2)^2}{2g_m(g_1 + g_2 + 2g_m)} < \epsilon, \quad (26)$$

from which it is seen that

$$g_m[\epsilon - \sqrt{\epsilon(\epsilon + 4|E_1|)}]/|E_1| < g_1 + g_2 < g_m[\epsilon + \sqrt{\epsilon(\epsilon + 4|E_1|)}]/|E_1|,$$

and relation 10 is implied because $\epsilon < \sqrt{\epsilon(\epsilon + 4|E_1|)}$.

Case II

$E_1 > 0 > E_2$. Supposing that $|E_1|g_1 > |E_2|g_2$, the error (Eq. 25) becomes

$$\frac{(g_1 + g_2)(|E_1|g_1 - |E_2|g_2)}{2g_m(g_1 + g_2 + 2g_m)} < \epsilon \quad (27)$$

by which one has

$$\frac{2\epsilon g_m + g_2(|E_2| - |E_1|) - \sqrt{[g_2(|E_1| + |E_2|) + 2\epsilon g_m]^2 + 16\epsilon|E_1|g_m^2}}{2|E_1|} < g_1 < \frac{2\epsilon g_m + g_2(|E_2| - |E_1|) + \sqrt{[g_2(|E_1| + |E_2|) + 2\epsilon g_m]^2 + 16\epsilon|E_1|g_m^2}}{2|E_1|}.$$

Because

$$2\epsilon g_m + g_2(|E_2| - |E_1|) < \sqrt{[g_2(|E_1| + |E_2|) + 2\epsilon g_m]^2 + 16\epsilon|E_1|g_m^2},$$

the lower bound is replaced such that

$$\frac{|E_2|g_2}{|E_1|} < g_1 < \frac{2\epsilon g_m + g_2(|E_2| - |E_1|) + \sqrt{[g_2(|E_1| + |E_2|) + 2\epsilon g_m]^2 + 16\epsilon|E_1|g_m^2}}{2|E_1|}. \quad (28)$$

Supposing, on the other hand, we have $|E_1|g_1 \le |E_2|g_2$, the error (Eq. 25) becomes

$$\frac{(g_1 + g_2)(|E_2|g_2 - |E_1|g_1)}{2g_m(g_1 + g_2 + 2g_m)} < \epsilon. \quad (29)$$

If $g_1 = 0$, which requires by Eq. 29 that $g_2 < g_m[\epsilon + \sqrt{\epsilon(\epsilon + 4|E_2|)}]/|E_2|$, we readily have Eq. 12. If $g_1 > 0$ or $g_2 \ge g_m[\epsilon + \sqrt{\epsilon(\epsilon + 4|E_2|)}]/|E_2|$, we must have $[g_2(|E_1| + |E_2|) - 2\epsilon g_m]^2 \ge 16\epsilon|E_1|g_m^2$. Because $g_2(|E_2| - |E_1|) - 2\epsilon g_m < \sqrt{[g_2(|E_1| + |E_2|) - 2\epsilon g_m]^2 - 16\epsilon|E_1|g_m^2}$ for sufficiently small ϵ, the error formula leads to

$$g_1 > \frac{g_2(|E_2| - |E_1|) - 2\epsilon g_m + \sqrt{[g_2(|E_1| + |E_2|) - 2\epsilon g_m]^2 - 16\epsilon|E_1|g_m^2}}{2|E_1|}.$$

This condition is consistent with the assumption that $|E_1|g_1 \le |E_2|g_2$ because

$$g_2(|E_1| + |E_2|) + 2\epsilon g_m \ge \sqrt{[g_2(|E_1| + |E_2|) - 2\epsilon g_m]^2 - 16\epsilon|E_1|g_m^2},$$

and one has

$$\frac{|E_2|g_2}{|E_1|} \ge g_1 > \frac{g_2(|E_2| - |E_1|) - 2\epsilon g_m + \sqrt{[g_2(|E_1| + |E_2|) - 2\epsilon g_m]^2 - 16\epsilon|E_1|g_m^2}}{2|E_1|}. \quad (30)$$

Combining Eqs. 28 and 30, we have Eq. 11.

A2. Dynamic range of multiplicative modes

The error formula is

$$\left|\frac{E_1 g_1 + E_2 g_2}{g_1 + g_2 + 2g_m} - \frac{E_2}{4g_m^2} g_1 g_2\right| = \frac{|4g_m^2(E_1 g_1 + E_2 g_2) - E_2 g_1 g_2(g_1 + g_2 + 2g_m)|}{4g_m^2(g_1 + g_2 + 2g_m)} < \epsilon. \tag{31}$$

Case I

$E_1 = E_2 \neq 0$. If $4g_m^2(g_1 + g_2) > g_1 g_2(g_1 + g_2 + 2g_m)$, the error becomes

$$\frac{|E_1|[4g_m^2(g_1 + g_2) - g_1 g_2(g_1 + g_2 + 2g_m)]}{4g_m^2(g_1 + g_2 + 2g_m)} < \epsilon,$$

which leads to

$$2|E_1|g_1 g_2 > 4g_m^2(|E_1| - \epsilon) - |E_1|g_2(g_2 + 2g_m) + \sqrt{[4g_m^2(|E_1| - \epsilon) - |E_1|g_2(g_2 + 2g_m)]^2 + 16|E_1|g_m^2 g_2[g_2(|E_1| - \epsilon) - 2\epsilon g_m]}. \tag{32}$$

If $4g_m^2(g_1 + g_2) \leq g_1 g_2(g_1 + g_2 + 2g_m)$, the error is

$$\frac{|E_1|[g_1 g_2(g_1 + g_2 + 2g_m) - 4g_m^2(g_1 + g_2)]}{4g_m^2(g_1 + g_2 + 2g_m)} < \epsilon,$$

from which one has

$$2|E_1|g_1 g_2 < 4g_m^2(|E_1| + \epsilon) - |E_1|g_2(g_2 + 2g_m) + \sqrt{[4g_m^2(|E_1| + \epsilon) - |E_1|g_2(g_2 + 2g_m)]^2 - 16|E_1|g_m^2 g_2[g_2(|E_1| + \epsilon) + 2\epsilon g_m]}. \tag{33}$$

Combining Eqs. 32 and 33 we have Eq. 14.

Case II

$E_1 > 0 > E_2$ (similar to Case I).

Case III

$E_1 = 0$, $E_2 \neq 0$ (similar to Case I).

A3. Dynamic range of divisive modes

For the case of $L = K = 1$, the error formula is:

$$\left|\frac{E_1 g_1 + E_2 g_2}{g_1 + g_2 + 2g_m} - \frac{E_2 g_2}{g_1 + 2g_m}\right| = \frac{|E_1 g_1(g_1 + 2g_m) - E_s g_2^2|}{(g_1 + g_2 + 2g_m)(g_1 + 2g_m)} \leq \epsilon. \tag{34}$$

Case I

$E_1 = E_2 \neq 0$. If $g_1(g_1 + 2g_m) > g_2^2$, or $g_1 > \sqrt{g_m^2 + g_2^2} - g_m$, the error (Eq. 34) becomes

$$\frac{|E_1|[g_1(g_1 + 2g_m) - g_2^2]}{(g_1 + g_2 + 2g_m)(g_1 + 2g_m)} \leq \epsilon.$$

This can be satisfied if

$$0 < g_1 < \frac{\epsilon(g_2 + 4g_m) - 2g_m|E_1| + \sqrt{[\epsilon g_2 + 2g_m|E_1|]^2 + 4|E_1|(|E_1| - \epsilon)g_2^2}}{2(|E_1| - \epsilon)}.$$

Therefore we have

$$\sqrt{g_m^2 + g_2^2} - g_m < g_1 < \frac{\epsilon(g_2 + 4g_m) - 2g_m|E_1| + \sqrt{[\epsilon g_2 + 2g_m|E_1|]^2 + 4|E_1|(|E_1| - \epsilon)g_2^2}}{2(|E_1| - \epsilon)}. \tag{35}$$

If $g_1(g_1 + 2g_m) \leq g_2^2$, or $g_1 \leq \sqrt{g_m^2 + g_2^2} - g_m$, the error (Eq. 34) becomes

$$\frac{|E_1|[g_2^2 - g_1(g_1 + 2g_m)]}{(g_1 + g_2 + 2g_m)(g_1 + 2g_m)} \leq \epsilon.$$

This leads to the condition that

$$g_1 > \frac{-[\epsilon(g_2 + 4g_m) + 2g_m|E_1|] + \sqrt{[2g_m|E_1| - \epsilon g_2]^2 + 4|E_1|(|E_1| + \epsilon)g_2^2}}{2(|E_1| + \epsilon)}.$$

Thus we have

$$\sqrt{g_m^2 + g_2^2} - g_m \geq g_1 > \frac{-[\epsilon(g_2 + 4g_m) + 2g_m|E_1|] + \sqrt{[2g_m|E_1| - \epsilon g_2]^2 + 4|E_1|(|E_1| + \epsilon)g_2^2}}{2(|E_1| + \epsilon)}. \tag{36}$$

Combining Eq. 36 with Eq. 35 we have Eq. 19.

Case II

$E_1 E_2 < 0$. The error Eq. 34 becomes

$$\frac{|E_1|g_1(g_1 + 2g_m) + |E_2|g_2^2}{(g_1 + g_2 + 2g_m)(g_1 + 2g_m)} \leq \epsilon$$

which results in Eq. 20 because

$$\epsilon(g_2 + 4g_m) - 2g_m|E_1| < \sqrt{[\epsilon g_2 + 2g_m|E_1|]^2 - 4|E_2|(|E_1| - \epsilon)g_2^2}$$

for small ϵ.

Case III

$E_1 = 0$ and $E_2 \neq 0$. The error (Eq. 34) is

$$\frac{|E_2|g_2}{(g_1 + g_2 + 2g_m)(g_1 + 2g_m)} < \epsilon$$

from which we readily have Eq. 21.

The authors are grateful to the reviewer for valuable comments and suggestions that have helped greatly in improving this work.

REFERENCES

Blomfield, S. 1974. Arithmetical operations performed by nerve cells. *Brain Res.* 69:115–124.

Carandini, M., and D. Heeger. 1994. Summation and division by neurons in primate visual cortex. *Science.* 264:1333–1336.

Dubin, R., and D. E. Rumelhart. 1990. Product units: a computationally powerful and biologically plausible extension to backpropagation networks. *Neural Computation.* 1:133–142.

Heeger, D. 1992. Normalization of cell responses in cat striate cortex. *Visual Neurosci.* 9:181–197.

Heeger, D. 1993. Modeling single-cell direction selectivity with normalized, half-squared, linear operators. *J. Neurophysiol.* 70:1885–1898.

Hubel, D., and T. Wiesel. 1962. Receptive fields, binocular interaction, and functional architecture in the cat's visual cortex. *J. Physiol. (Lond.).* 160:106–154.

Kandel, E. R., J. H. Schwartz, and T. M. Jessell. eds. 1991. *Principles of Neural Science,* 3rd ed. Elsevier, New York.

Koch, C., and T. Poggio. 1992. Multiplying with synapses and neurons. *In Single Neuron Computation.* T. McKenna, J. Davis, and S. F. Zornetzer, editors. Academic Press, Inc., Boston. 315–345.

Koch, C., T. Poggio, and V. Torre. 1982. Retinal ganglion cells: a functional interpretation of dendritic morphology. *Philos. Trans. R. Soc. Lond Biol. Sci.* 298:227–264.

Marr, D. 1970. A theory for cerebral neocortex. *Proc. R. Soc. Lond. Biol. Sci.* 176:161–234.

Mel, B. W. 1994. Information processing in dendritic trees. *Neural Computation.* 6:1031–1085.

Mel, B. W., and C. Koch. 1990. Sigma-pi learning: on radial basis functions and cortical associative learning. *In*Long. Advances in Neural Information Processing Systems, Vol. 2. D. S. Touretzky, editor, Morgan Kaufmann, San Mateo, CA. 474–481.

Poggio, T., and F. Girosi. 1990. Regularization algorithms for learning that are equivalent to multilayer networks. *Science.* 247:978–982.

Poggio, T., and V. Torre. 1981. A theory of synaptic interactions. *In* Theoretical Approaches in Neurobiology. W. E. Reichardt and T. Poggio, editors. MIT Press, Cambridge, MA. 28–38.

Shepherd, G. M., and R. K. Brayton. 1987. Logic operations are properties of computer-simulated interactions between excitable dendritic spines. *Neuroscience.* 21:151–166.

Torre, V., and T. Poggio. 1978. A synaptic mechanism possibly underlying directional selectivity to motion. *Proc. R. Soc. Lond. Biol. Sci.* 202: 409–416.

Zador, A. M., B. J. Claiborne, and T. J. Brown. 1992. Nonlinear pattern separation in single hippocampal neurons with active dendritic membrane. *In* Advances in Neural Information Processing Systems, Vol. 4. J. Moody, S. Hanson, and R. Lippmann, editors. Morgan Kaufmann, San Mateo, CA. 51–58.